Analysis of a 2D neural field equation with finite transmission speed

Kevin Green, Axel Hutt

Technical Report: Analysis of a 2D neural field equation with finite transmission speed

Kevin R. Green[1] and A. Hutt

INRIA Nancy Grand-Est, team NEUROSYS, Villers-lés-Nancy, France

2014-02-01 to 2014-05-31

[1]kevin.green@uoit.ca

Contents

Chapter 1

Model specification

1.1 General model

We begin simply by writing a general expression for a continuum model for the propagation of electrical activity in neural tissue in two dimensions,

$$u(\mathbf{x},t) = \int_{-\infty}^{t} \mathrm{d}t'\, \eta\left(t,t'\right) \left(\int_{\Omega} \mathrm{d}\mathbf{x}'\, w\left(\mathbf{x}-\mathbf{x}'\right) f\left[u\left(\mathbf{x}', t' - \frac{\|\mathbf{x}-\mathbf{x}'\|}{v} \right) \right] + p(\mathbf{x},t') \right). \tag{1.1}$$

This form of equation can be obtained by a straightforward generalization of one dimensional models that arise when considering a single population of identical neurons [1–3]. An example of how to go from a physiologically motivated model to this form is given in the next section.

Here, $u(\mathbf{x},t)$ represents the synaptic activity of the neurons at position $\mathbf{x} \in \Omega \subseteq \mathbb{R}^2$ and at time $t \in [0,\infty)$. The firing rate function f converts the local synaptic activity to a firing rate. For example, if one considers a population of all-or-nothing neurons with a mean and standard deviation of firing rates, then f can be formally defined in terms of the error function, as in Hutt and Atay [4], however it is often written as some other symmetrical sigmoidal function for simplicity, as in Wilson and Cowan [5].

The strength of synaptic connections at position $\mathbf{x}$ is given by the connection density $w(\mathbf{x})$, which also incorporates the sign of the synaptic coupling for excitatory and inhibitory interaction. To simplify matters in this report, w is taken to be homogeneous and isotropic, such that $w(\mathbf{x}) = w(\|\mathbf{x}\|)$. While this is in general not a good assumption for connections in, say, the V1 cortex, we are attempting to show novel results for the two-dimensional field, and our first efforts greatly benefit from this simplifying assumption. Work on one-dimensional neural fields with inhomogeneous connections exists, in particular spatially periodic modulation of the connectivity is shown to alter the behaviour of waves [6,7], and it is likely that further work in two dimensions can follow a similar route.

The temporal convolution involving $\eta(t,t')$ represents the synaptic integration of signals within the network and is called the synaptic response kernel. Written in this way, η can be considered as a Green's function for some temporally invariant linear operator $\hat{L}$

$$\hat{L}\eta(t,t') = \hat{L}\eta(t-t') = \delta(t-t'). \tag{1.2}$$

This allows us to rewrite eq. (1.1) in the equivalent form

$$\hat{L}u(\mathbf{x},t) = \int_{\Omega} \mathrm{d}\mathbf{x}'\, w\left(\mathbf{x}-\mathbf{x}'\right) f\left[u\left(\mathbf{x}', t' - \frac{\|\mathbf{x}-\mathbf{x}'\|}{v} \right) \right] + p(\mathbf{x},t'). \tag{1.3}$$

The delayed temporal argument to u within the spatial integration, $t' - \|\mathbf{x} - \mathbf{x}'\|/v$, represents the delay incurred by signals travelling from position $\mathbf{x}'$ to $\mathbf{x}$ with speed v, $\|\cdot\|$ being the L_2-norm. And finally, external synaptic input to the model is represented by $p(\mathbf{x}, t)$.

If we define the spatio-temporal connectivity kernel K,

$$K(\mathbf{x}, t) = w(\mathbf{x})\delta\left(t - \|\mathbf{x}\|/v\right), \tag{1.4}$$

then we can rewrite eq. (1.1) in a compact convolution notation

$$u(\mathbf{x}, t) = \eta * \left(K \otimes f \circ u + p\right), \tag{1.5}$$

with the temporal convoution defined as

$$\left(\eta * h\right)(t) = \int_{-\infty}^{t} \mathrm{d}s\, \eta(t - s)h(s), \tag{1.6}$$

and a spatio-temporal convolution defined as

$$\left(K \otimes g\right)(\mathbf{x}, t) = \int_{-\infty}^{\infty} \mathrm{d}t' \int_{\mathbb{R}^2} \mathrm{d}\mathbf{x}'\, K\left(\mathbf{x} - \mathbf{x}', t - t'\right) g\left(\mathbf{x}', t'\right), \tag{1.7}$$

For the remainder of the report, the model as defined in either of eqs. (1.3) or (1.5) will be used when general results are desired, but when specific computations are required, the next section outlines properties of some specific functions to use for the elements of the model – η, ω (K), and f.

1.2 A specific model

1.2.1 Specific kernels

Starting with Hutt et al. [8] and their analysis of a one dimensional neural field with delay, we can make the same assumptions on the neural populations for the two dimensional case. These assumptions include[1]:

- identical impulse response functions for excitatory and inhibitory response $\eta(t - \tau)$, and identical firing functions f
- common propagation speed for both excitatory and inhibitory intracortical connections v
- homogeneous isotropic connections $w(\mathbf{x}) = w(\|\mathbf{x}\|)$

This generalization to two dimensions is straightforward up until their eq. (4), which we write in the general form

$$u(\mathbf{x}, t) = \int_{-\infty}^{t} \mathrm{d}\tau\, \eta(t - \tau) \times \left\{ \int_{\Omega} \mathrm{d}\mathbf{x}' \left(a_e h_e(\mathbf{x}, \mathbf{x}') - a_i h_i(\mathbf{x}, \mathbf{x}')\right) f\left[u\left(\mathbf{x}', \tau - \frac{\|\mathbf{x} - \mathbf{x}'\|}{v}\right)\right] + p(\mathbf{x}', \tau) \right\}. \tag{1.8}$$

[1] Note the difference in notation from [8]

The main differences being that now $\mathbf{x} \in \Omega$ is two dimensional, and we use the Euclidean norm $\|\mathbf{x}\| = \|\mathbf{x}\|_2 = \sqrt{x_1^2 + x_2^2}$ for distance.

For the synaptic response kernel, we take a function with two exponentially decaying time scales, such as

$$\eta(t) = \frac{\alpha_1 \alpha_2}{\alpha_2 - \alpha_1} \left(e^{-\alpha_1 t} - e^{-\alpha_2 t} \right) \Theta(t), \tag{1.9}$$

with $\Theta(t)$ the Heaviside step function. This results in the linear operator

$$\hat{L} = \left(\frac{1}{\alpha_1} \frac{\partial}{\partial t} + 1 \right) \left(\frac{1}{\alpha_2} \frac{\partial}{\partial t} + 1 \right) \tag{1.10}$$

according to the property listed in eq. (1.2).

Now, when it comes to the connection probability functions, we will use the exponentially decaying homogeneous and isotropic connections as in the one dimensional case, but when normalized in $\mathbb{R}^2$ we have

$$h_j(\mathbf{x}, \mathbf{x}') = \frac{1}{2\pi r_j^2} e^{-\|\mathbf{x} - \mathbf{x}'\|/r_j}, \quad j \in (e, i), \tag{1.11}$$

and finally a_e and a_i positive constants determining the strength of excitatory and inhibitory connections respectively.

Subbing these into eq. (1.8) and nondimensionalizing in the same way as in [8], i.e., $t \to t\sqrt{\alpha_1 \alpha_2}$, $\mathbf{x} \to \mathbf{x}/r_e$, $v \to v/(r_e\sqrt{\alpha_1 \alpha_2})$, we obtain

$$\left(\frac{\partial^2}{\partial t^2} + \alpha \frac{\partial}{\partial t} + 1 \right) u(\mathbf{x}, t) = \frac{1}{2\pi} \int_\Omega \mathrm{d}\mathbf{x}' \left(a_e e^{-\|\mathbf{x} - \mathbf{x}'\|} - a_i r^2 e^{-r\|\mathbf{x} - \mathbf{x}'\|} \right) f \left[u \left(\mathbf{x}', t - \frac{\|\mathbf{x} - \mathbf{x}'\|}{v} \right) \right] + p(\mathbf{x}, t), \tag{1.12}$$

with

$$\alpha = \frac{\alpha_1 + \alpha_2}{\sqrt{\alpha_1 \alpha_2}}. \tag{1.13}$$

Thus, in the general form written in eq. (1.5), we can take the temporal kernel as in eq. (1.9), the spatio-temporal kernel as

$$K(\mathbf{x}, t) = \frac{1}{2\pi} \left(a_e e^{-\|\mathbf{x}\|} - a_i r^2 e^{-r\|\mathbf{x}\|} \right) \delta(t - \|\mathbf{x}\|/v), \tag{1.14}$$

and a standard sigmoid for the firing rate function

$$f[u] = \frac{f_{max}}{1 + e^{-C(u - \theta)}}, \tag{1.15}$$

where f_{max} is the maximum firing rate, θ sets the firing threshold, and C the steepness at threshold, to work with a physiologically relevant version of the general equation.

1.2.2 Transforms of specific kernels

Analysis of the general form, eq. (1.5), can be simplified by looking at certain integral transforms of the different elements of the model. However, this often results in a dense notation that needs to be unpacked for actual numerical analysis or understanding of the results. This subsection states the necessary transforms for a specific instance of the synaptic response kernel and the spatio-temporal connectivity kernel.

Laplace transform of temporal kernel

Defining the Laplace transform as

$$\tilde{\eta}(\lambda) = \int_0^\infty \mathrm{d}s\, \eta(s) e^{-\lambda s}, \tag{1.16}$$

we compute the Laplace transform of the specific η defined by eq. (1.9) as

$$\tilde{\eta}(\lambda) = \frac{1}{(\lambda^2 + \alpha\lambda + 1)}, \tag{1.17}$$

with α as in eq. (1.13).

Fourier-Laplace of spatio-temporal kernel

Defining the Fourier-Laplace transform as

$$\widehat{K}(\mathbf{k}, \lambda) = \int_{\mathbb{R}^2} \mathrm{d}\mathbf{y} \int_0^\infty \mathrm{d}s\, K(\mathbf{y}, s) e^{-(i\mathbf{k}\cdot\mathbf{y} + \lambda s)}, \tag{1.18}$$

we compute the Fourier-Laplace transform of the specific K defined by eq. (1.14) as

$$\widehat{K}(\mathbf{k}, \lambda) = \frac{1 + \lambda/v}{\left((1 + \lambda/v)^2 + k^2\right)^{3/2}} a_e - \frac{r + \lambda/v}{\left((r + \lambda/v)^2 + k^2\right)^{3/2}} r^2 a_i, \tag{1.19}$$

with $k = \|\mathbf{k}\| = \sqrt{k_1^2 + k_2^2}$. For any homogeneous isotropic kernel, it will be the case that the Fourier-Laplace transform will depend only on the magnitude of $\mathbf{k}$ squared. The only reason we don't write it explicitly as such is that keeping the vector argument helps structure calculations in chapter 4. The computation of eq. (1.19) relies on identities such as eq. (9.1.21) in Abramowitz and Stegun [9] and eq. (6.621.4) in Gradshteyn [10].

Fourier transform of moments of connectivity kernel

In perturbative analysis of the model, we will see that solutions can be expressed in terms of the Fourier transform of moments of the connectivity kernel,

$$\widehat{w}_n(\mathbf{k}) = \int_{\mathbb{R}^2} \mathrm{d}\mathbf{x}\, \|\mathbf{x}\|^n w(\mathbf{x})\, e^{-i\mathbf{k}\cdot\mathbf{x}}. \tag{1.20}$$

To summarize, the first few are given by

$$\widehat{w}_0(\mathbf{k}) = \widehat{K}(\mathbf{k}, 0) = \frac{a_e}{(1 + k^2)^{3/2}} - \frac{r^3 a_i}{(r^2 + k^2)^{3/2}} \tag{1.21}$$

$$\widehat{w}_1(\mathbf{k}) = \left(\frac{3}{1 + k^2} - 1\right) \frac{a_e}{(1 + k^2)^{3/2}} - \left(\frac{3r^2}{r^2 + k^2} - 1\right) \frac{r^2 a_i}{(1 + k^2)^{3/2}} \tag{1.22}$$

$$\widehat{w}_2(\mathbf{k}) = \left(9 - \frac{15}{1 + k^2}\right) \frac{a_e}{(1 + k^2)^{5/2}} - \left(9 - \frac{15r^2}{r^3 + k^2}\right) \frac{r^2 a_i}{(r^2 + k^2)^{5/2}} \tag{1.23}$$

again with special function integrals found in [9, 10].

1.2.3 Simulation considerations

Exponentially decaying connection densities are easily normalized when looking at $\mathbb{R}^2$, but when we move to the periodic square $\Omega = [-L/2, L/2] \times [-L/2, L/2]$, the normalization constants can only be reduced to integrals that must be solved numerically. As this is the domain used in simulation code such as [11], which is based on the numerical scheme from [12], we need to understand when and how it will differ from analysis on the infinite domain.

Additional numerical constants can be added to the model in such a way that the homogeneous equilibrium will be the same for both the infinite domain and this finite periodic domain.

A simple condition for the minimal system size L_{min} for a given numerical precision ϵ that allows this normalization to be as if the system were infinite is derived.

Normalization

Starting from the exponential connectivity,

$$h(\mathbf{x}) = \frac{r^2}{2\pi N} e^{-r\|\mathbf{x}\|}, \tag{1.24}$$

we seek to find N such that

$$\int_\Omega \mathrm{d}\mathbf{x}\, h(\mathbf{x}) = 1 \tag{1.25}$$

with $\Omega = [-L/2, L/2] \times [-L/2, L/2]$.

Due to symmetry of this integrand, we can express this in terms of an integral over a triangle

$$\frac{4r^2}{\pi N} \int_0^{L/2} \mathrm{d}x_1 \int_0^{x_1} \mathrm{d}x_2\, e^{-r\sqrt{x_1^2+x_2^2}} = 1, \tag{1.26}$$

which can be re-written in polar coordinates.

$$\frac{4r^2}{\pi N} \int_0^{\pi/4} \mathrm{d}\varphi \int_0^{\frac{L}{2}\sec\varphi} \mathrm{d}\rho\, \rho e^{-r\rho} = 1. \tag{1.27}$$

The integral over ρ can be evaluated, but the remaining integral can not (in terms of elementary functions). Rearranging the result for N, we obtain

$$N = 1 - \frac{2}{\pi} Lr \int_0^{\pi/4} \sec\varphi e^{-\frac{L}{2}\sec\varphi} \mathrm{d}\varphi - \frac{4}{\pi} \int_0^{\pi/4} e^{-\frac{L}{2}\sec\varphi} \mathrm{d}\varphi \tag{1.28}$$

The above was formulated in such a way that would allow us to write the model equation as

$$\hat{L}u(\mathbf{x},t) = \left(\frac{\partial^2}{\partial t^2} + \alpha\frac{\partial}{\partial t} + 1\right) u(\mathbf{x},t) = \\ \frac{1}{2\pi} \int_\Omega \mathrm{d}\mathbf{x}' \left(\frac{a_e}{N_e} e^{-\|\mathbf{x}-\mathbf{x}'\|} - \frac{a_i}{N_i} r^2 e^{-r\|\mathbf{x}-\mathbf{x}'\|}\right) f\left[u\left(\mathbf{x}', t - \frac{\|\mathbf{x}-\mathbf{x}'\|}{v}\right)\right] + p(\mathbf{x},t), \tag{1.29}$$

where

$$N_e = 1 - \frac{2}{\pi} L \int_0^{\pi/4} \sec\varphi e^{-\frac{L}{2}\sec\varphi} \mathrm{d}\varphi - \frac{4}{\pi} \int_0^{\pi/4} e^{-\frac{L}{2}\sec\varphi} \mathrm{d}\varphi \tag{1.30}$$

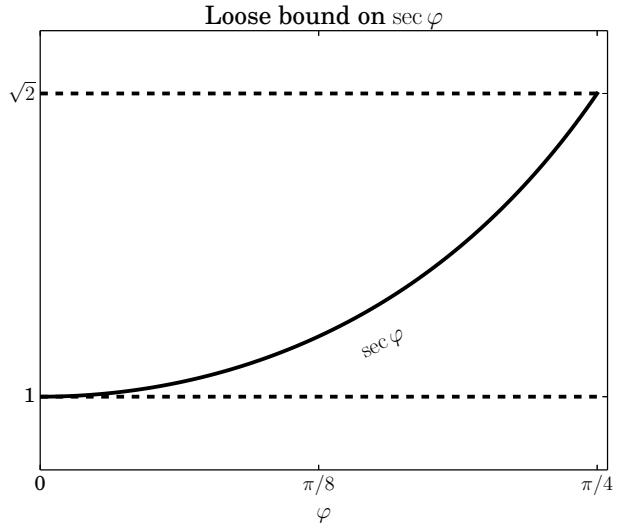

Figure 1.1: Visualization of some loose bounds for $\sec\varphi$.

$$N_i = 1 - \frac{2}{\pi} Lr \int_0^{\pi/4} \sec\varphi e^{-\frac{Lr}{2}\sec\varphi} \mathrm{d}\varphi - \frac{4}{\pi} \int_0^{\pi/4} e^{-\frac{Lr}{2}\sec\varphi} \mathrm{d}\varphi. \tag{1.31}$$

Comparison of eq. (1.29) to eq. (1.12) makes it clear that due to this normalization issue, the model parameters in numerical simulation,

$$\tilde{a_e} = \frac{a_e}{N_e}, \quad \tilde{a_i} = \frac{a_i}{N_i}, \tag{1.32}$$

can be different from what one is expecting if the domain is not large enough.

Normalized up to a given precision

The integrals in eqs. (1.30) and (1.31), while not able to be evaluated explicitly, can be bounded by noting that

$$N_j = 1 - I_j, \quad I_j > 0, \quad j \in (e, i). \tag{1.33}$$

That is, if we can find an L such that $I_j < \epsilon$, where ϵ is our numerical precision, then we can be justified in using the same paramaters in both the infinite domain analysis and the numerical simulation.

This can be done most simply by noting the bounds

$$1 \leq \sec\varphi \leq \sqrt{2}, \quad \varphi \in [0, \pi/4], \tag{1.34}$$

seen in fig. 1.1, which allow us to write (for I_i in particular)

$$I_i \leq \frac{2}{\pi} Lr \int_0^{\pi/4} \sqrt{2} e^{-Lr/2} \,\mathrm{d}\varphi + \frac{4}{\pi} \int_0^{\pi/4} e^{-Lr/2} \,\mathrm{d}\varphi \tag{1.35}$$

which is very easy to evaluate

$$I_i \leq \left(\frac{1}{\sqrt{2}} Lr + 1 \right) e^{-Lr/2}. \tag{1.36}$$

Finally, taking I_i to be in strict equality with ϵ results in

$$\epsilon e^{L_i r/2} - \left(\frac{1}{\sqrt{2}} L_i r + 1\right) = 0. \tag{1.37}$$

Solving this transcendental equation (which has a unique solution, $L_i > 0$) results in the minimal L_i that allows for $N_i \approx 1$ up to precision ϵ.

The more general case for this model, since there are two length scales, is to take the minimum simulation size

$$L_{min} = \max\left(L_e, L_i\right) = \begin{cases} L_e & r > 1 \\ L_i & r < 1 \end{cases} \tag{1.38}$$

with L_e determined by

$$\epsilon e^{L_e/2} - \left(\frac{1}{\sqrt{2}} L_e + 1\right) = 0. \tag{1.39}$$

The choice between the two values simply depends on the possibilities $r < 1$ and $r > 1$.

If we consider double precision arithmetic, $\epsilon \sim 2.22 \times 10^{-16}$, and $r > 1$, then eq. (1.38), says we should take $L \geq 39.4063$ to gaurantee that the normalization of the exponentials does not affect our parameters.

Tighter bound

A more accurate equation can be easily derived using $1 \leq \sec\varphi \leq 4(\sqrt{2}-1)\varphi/\pi + 1$ as in fig. 1.2. This also results in transcendental equations with unique solutions to be solved. We still use eq. (1.38) to determine the minimum length of the system, but now L_e and L_i come from

$$\epsilon e^{L_e/2} - \left(\frac{1}{4}\left(\sqrt{2}-1\right) L_e + \frac{3}{2}\right) = 0, \tag{1.40}$$

$$\epsilon e^{L_i r/2} - \left(\frac{1}{4}\left(\sqrt{2}-1\right) L_i r + \frac{3}{2}\right) = 0. \tag{1.41}$$

Looking at double precision again with $r > 1$, this produces the minimum length $L \geq 37.7314$. Further refinement on the bounds will produce ever better estimates for the minimum system size, or quadrature in combination with root finding can even be applied to the integral equations to avoid this bounding argument.

Other effects of finite size

The above discussion has ignored other terms that arise from the analysis on a finite square. These however can be reduced to integrals of exponential order as well, and a similar argument to that used in the normalization constants can be used to ignore them.

On the periodic square, regardless of how large, the finite size serves to discretize the spectrum to $\mathbf{k}_{nm} = (k_n, k_m)^T$, with a resolution given by

$$\Delta k = k_{n+1} - k_n = \frac{2\pi}{L}. \tag{1.42}$$

With $L = 37.7314$ as above, this gives $\Delta k = 0.1665\ldots$. It will be seen in Chapter 3 that dynamic Turing bifurcations seem only to occur for large wavenumbers ($k > 1$), so trying to simulate results

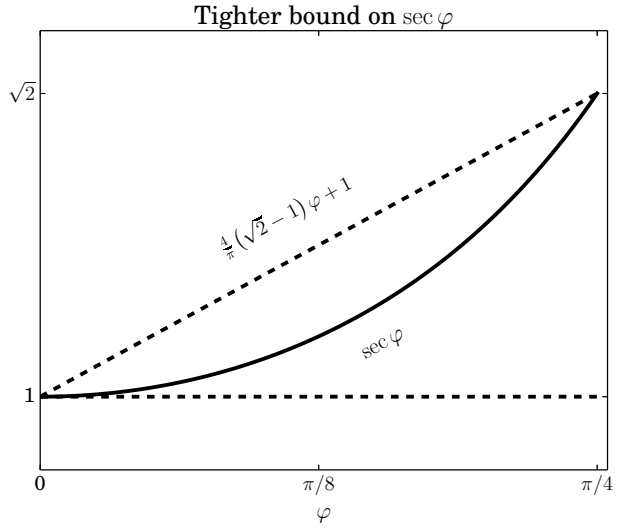

Figure 1.2: Visualization of some tighter bounds for $\sec\varphi$. The integrals with this bound reduce to transcendental equations with a unique solution.

near these bifurcations will require a domain that contains many wavelengths of the bifurcating modes, while the analysis in Chapter 4 is based on single wavelengths (that is to say, extra care has to be taken when comparing to simulation).

This discretization is also justified because of its dependence on L. That is to say, that we can ignore the effects of the exponential integrals $\sim e^{-L}$ before we can ignore the discretization of the spectrum due to $\sim k^2 \sim L^{-2}$ for large L.

Chapter 2

Starting from equilibria

This chapter will build up some dynamical analysis, starting from spatially homogeneous equilibra. Linearization about such equilibria is followed by a definition of the spectrum, and finally some basic description and analysis of bifurcations is presented.

2.1 Spatially homogeneous equilibrium

Consider a constant, spatially homogeneous external input $p(\mathbf{x}, t) = p_0$ to the model eq. (1.5). It can be shown that a spatially homogeneous solution u_0 will exist satisfying

$$u_0 = \tilde{\eta}(0)\left(\widehat{K}(0,0)f(u_0) + p_0\right), \tag{2.1}$$

where we have defined the Laplace and Fourier-Laplace integral transforms according to eqs. (1.16) and eq. (1.18).

To analyze the stability of an equilibrium u_0, we need to derive the first variational equation of eq. (1.5). This is accomplished by Taylor expanding the firing rate function to

$$f(u) = f(u_0) + \gamma_1 (u - u_0) + \mathcal{O}\left((u - u_0)^2\right), \tag{2.2}$$

with $\gamma_1 = f'(u_0)$ and taking

$$u(\mathbf{x}, t) - u_0 = \epsilon\, U(\mathbf{x}, t). \tag{2.3}$$

Subbing this linear perturbation into eq. (1.5) results in (after cancellation due to eq. (2.1))

$$U = \gamma_1 \eta * K \otimes U \tag{2.4}$$

as the first variational equation for the general model.

For the dispersion relation, we look at solutions to eq. (2.4) of the form

$$U(\mathbf{x}, t) = \int \mathrm{d}\mathbf{k}\, \widehat{U}(\mathbf{k}) e^{i\mathbf{k}\cdot\mathbf{x} + \lambda(k)t}. \tag{2.5}$$

Subbing this in, and using the definitions of the Laplace and Fourier-Laplace transforms allows us to write

$$L(\mathbf{k}, \lambda) = 1 - \gamma_1 \tilde{\eta}(\lambda)\widehat{K}(\mathbf{k}, \lambda) = 0. \tag{2.6}$$

And for the specific kernels defined earlier, the dispersion relation works out to

$$\lambda^2 + \alpha\lambda + 1 - \gamma_1 \left[\frac{1 + \lambda/v}{((1 + \lambda/v)^2 + k^2)^{3/2}} a_e - \frac{r + \lambda/v}{((r + \lambda/v)^2 + k^2)^{3/2}} r^2 a_i\right] = 0. \tag{2.7}$$

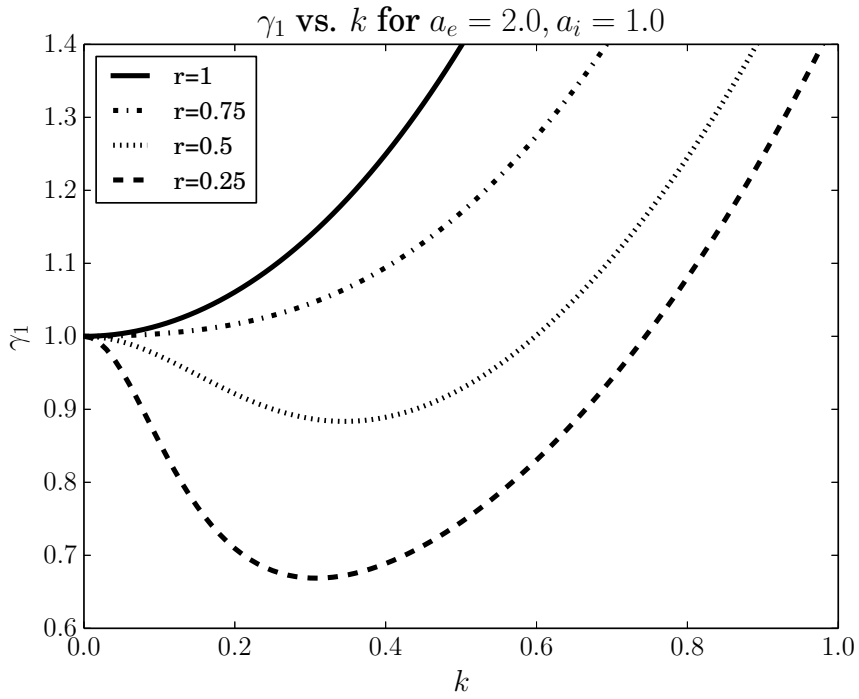

Figure 2.1: Visualization of eq. (2.8). When the curve permits a minimum at $k_c > 0$, the system can undergo a Turing bifurcation [13] to modes where the norm of the wavevector is k_c.

2.2 Stationary bifurcation

We can look at monotonic and wave instabilities of the equilibria by looking at specific values of the growth rate λ. First, for monotonic instabilities, we set $\lambda = 0$, which allows us to write, in general,

$$L(\mathbf{k}, 0) = 0, \tag{2.8}$$

and for our specific kernels,

$$\frac{1}{\gamma_1} = \left[\frac{a_e}{(1+k^2)^{3/2}} - \frac{r^3 a_i}{(r^2+k^2)^{3/2}} \right], \tag{2.9}$$

which we can see does not depend in any way on the transmission speed v. From this equation, we plot γ_1 vs. k for various values of r in fig. 2.1. We can also look at how k_c, the minimum of the curve, changes with r, as in fig. 2.2. Finally, we plot the value of γ_1 required for a Turing bifurcation in fig. 2.3. Brief descriptions of how to interpret the figures are given in their captions. And setting $k = 0$ as well, to check for the homogeneous state perturbation, we obtain

$$\gamma_1 = \frac{1}{a_e - a_i}, \tag{2.10}$$

for which we have stability of u_0 for

$$\gamma_1 < \frac{1}{a_e - a_i}, \tag{2.11}$$

which is the same for the one-dimensional case [8].

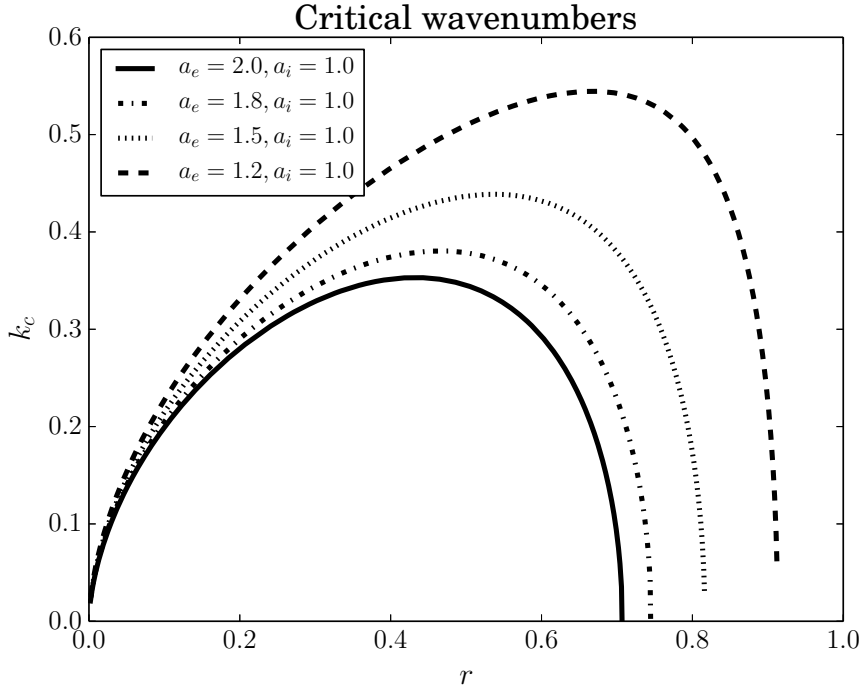

Figure 2.2: The mode responsible for Turing bifurcation, as a function of r.

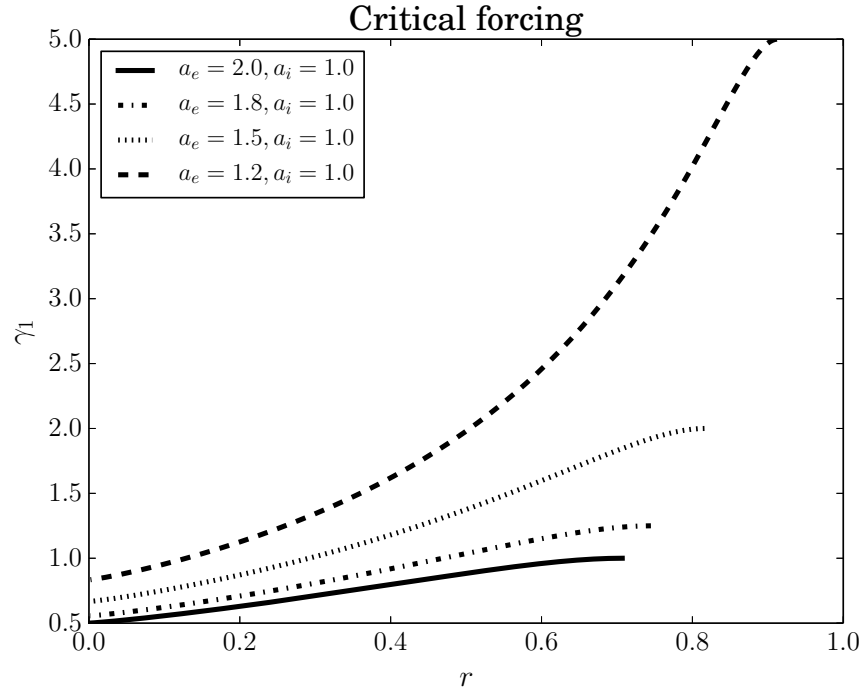

Figure 2.3: Turing bifurcations occur on the lines.

2.3 Nonstationary bifurcation

To look at the wave instability we start by splitting λ into real and imaginary parts, $\lambda = \mu + i\omega$ in eq. (2.6)

$$L(\mathbf{k}, \mu + i\omega) = 0, \tag{2.12}$$

which for the specific kernel results in

$$\begin{aligned}(\mu + i\omega)^2 + \alpha\,(\mu + i\omega) + 1 = \\ \gamma_1 \left[\frac{1 + (\mu + i\omega)/v}{((1 + (\mu + i\omega)/v)^2 + k^2)^{3/2}} a_e - \frac{r + (\mu + i\omega)/v}{((r + (\mu + i\omega)/v)^2 + k^2)^{3/2}} r^2 a_i \right].\end{aligned} \tag{2.13}$$

Defining the quantities

$$R_r = \sqrt{(r^2 + k^2 - \omega^2/v^2)^2 + (2\omega/v)^2 r^2}, \tag{2.14}$$

$$\theta_r = \arctan \frac{2\omega r/v}{r^2 + k^2 - \omega^2/v^2}, \tag{2.15}$$

allows the denominators to be written in terms of complex exponentials $R^{-3/2} e^{-i3\theta/2}$. Expanding these in terms of sin and cos and extracting the real and the imaginary parts, gives two equations

$$\begin{aligned}\frac{\mu^2 + \alpha\mu + 1 - \omega^2}{\gamma_1} = \left[\left(\cos\left(\frac{3}{2}\theta_{1+\mu/v}\right) + \frac{\omega}{v} \sin\left(\frac{3}{2}\theta_{1+\mu/v}\right) \right) a_e R_{1+\mu/v}^{-3/2} - \right. \\ \left. \left(r \cos\left(\frac{3}{2}\theta_{r+\mu/v}\right) - \frac{\omega}{v} \sin\left(\frac{3}{2}\theta_{r+\mu/v}\right) \right) a_i r^2 R_{r+\mu/v}^{-3/2} \right],\end{aligned} \tag{2.16}$$

$$\begin{aligned}\frac{(2\mu + \alpha)\,\omega}{\gamma_1} = \left[\left(\frac{\omega}{v} \cos\left(\frac{3}{2}\theta_{1+\mu/v}\right) - \sin\left(\frac{3}{2}\theta_{1+\mu/v}\right) \right) a_e R_{1+\mu/v}^{-3/2} - \right. \\ \left. \left(\frac{\omega}{v} \cos\left(\frac{3}{2}\theta_{r+\mu/v}\right) - r \sin\left(\frac{3}{2}\theta_{r+\mu/v}\right) \right) a_i r^2 R_{r+\mu/v}^{-3/2} \right],\end{aligned} \tag{2.17}$$

noting the various subscripts on R and θ.

And finally, setting $\mu = 0$ gives two very nonlinear equations (in ω) that must be satisfied for a Hopf bifurcation to occur. In general,

$$\begin{aligned}\operatorname{Re} L\,(\mathbf{k}, i\omega) = 0, \\ \operatorname{Im} L\,(\mathbf{k}, i\omega) = 0,\end{aligned} \tag{2.18}$$

and for our specific kernels these are

$$\begin{aligned}\frac{1 - \omega^2}{\gamma_1} = \left[\left(\cos\left(\frac{3}{2}\theta_1\right) + \frac{\omega}{v} \sin\left(\frac{3}{2}\theta_1\right) \right) a_e R_1^{-3/2} - \right. \\ \left. \left(r \cos\left(\frac{3}{2}\theta_r\right) - \frac{\omega}{v} \sin\left(\frac{3}{2}\theta_r\right) \right) a_i r^2 R_r^{-3/2} \right],\end{aligned} \tag{2.19}$$

$$\begin{aligned}\frac{(\alpha + 1/\alpha)\omega}{\gamma_1} = \left[\left(\frac{\omega}{v} \cos\left(\frac{3}{2}\theta_1\right) - \sin\left(\frac{3}{2}\theta_1\right) \right) a_e R_1^{-3/2} - \right. \\ \left. \left(\frac{\omega}{v} \cos\left(\frac{3}{2}\theta_r\right) - r \sin\left(\frac{3}{2}\theta_r\right) \right) a_i r^2 R_r^{-3/2} \right].\end{aligned} \tag{2.20}$$

Because of the $\sin(3\theta_r/2)$ and $\cos(3\theta_r/2)$ pieces, and our ability to write θ_r in terms of either arcsin or arccos, we can apply half- and triple-angle formulae to eliminate the trigonometric dependence of these equations, at the expense of replacing them with even worse looking radicals.

This is much worse to deal with than the polynomials that arise in the 1D case as in [8]. So much worse that it might be worth it to look at an extension of the asymptotic results of Atay and Hutt [14] to two dimensions, and consider large finite transmission speeds.

Actually, taking the approach of Hutt and Atay [4] to derive some necessary conditions for wave-mode instabilities for general v extends easily to the two-dimensional field as well. While the necessary conditions allow us to find parameter sets where we are guaranteed to have an equilibrium with some part of the spectrum crossing the imaginary axis, they offer no information about how the wave instability sets in, or even the range of oscillatory modes that are unstable for a given parameter set. To get this information, we need to look at eqs. (2.19) and (2.20) numerically, which is what is presented in the next chapter.

Chapter 3

Numerically computing linear spectrum

This chapter looks to analyze the characteristic equation that comes up from the field equation in two dimensions. Analyzing the equation here is more involved than in the one-dimensional case because the equation involves irreducible radicals of the eigenvalue λ. The approach taken is to find all of the roots of the dispersion relation for $k = 0$ and then perform numerical continuation in k.

With the spectrum computed this way, we move on to an extended system that allows us to continue critical points in the spectrum, corresponding to (potential) Turing and Turing-Hopf bifurcations. Finally, with the Turing and Turing-Hopf bifurcations computed, we can perform a continuation of them by taking a different view of the extended system.

3.1 Roots of the $k = 0$ case

Recall from the previous chapter the dispersion relation with the specific kernels, eq. (2.7).

We will first look at the solutions of eq. (2.7) as $\lambda = \lambda_j(p, k) \in \mathbb{C}$, where the subscript j indicates distinct spectral curves, and p the set of parameters. We immediately rewrite this in the form

$$\begin{aligned} F(\lambda, k, p) = &\left[(1+\lambda/v)^2 + k^2\right]^{3/2} \left[(r+\lambda/v)^2 + k^2\right]^{3/2} \left(\lambda^2 + \alpha\lambda + 1\right) - \\ &\gamma_1 \left[(1+\lambda/v)\left[(r+\lambda/v)^2 + k^2\right]^{3/2} a_e - (r+\lambda/v)\left[(1+\lambda/v)^2 + k^2\right]^{3/2} a_i r^2\right] = 0, \end{aligned} \tag{3.1}$$

We start by setting $k = 0$, and immediately notice the following issue in simplifying the radicals

$$\left((r+\lambda/v)^2\right)^{3/2} = \pm (r+\lambda/v)^3 . \tag{3.2}$$

Taking into account both places where this turns up, we choose to write the homogeneous system as

$$P(A, B, \lambda) = (1+\lambda/v)^2 (r+\lambda/v)^2 \hat{L}(\lambda) - \gamma_1 \left[A (r+\lambda/v)^2 a_e - B (1+\lambda/v)^2 a_i r^2\right] = 0, \tag{3.3}$$

and look at the 4 different polynomials given by

$$\begin{aligned} P_1(\lambda) &= P(1,1,\lambda), \\ P_2(\lambda) &= P(1,-1,\lambda), \\ P_3(\lambda) &= P(-1,1,\lambda), \\ P_4(\lambda) &= P(-1,-1,\lambda). \end{aligned} \tag{3.4}$$

We find all roots of each of these polynomials $\{\lambda_{nm} | P_n(\lambda_m) = 0\}$, and keep the roots that satisfy $F(\lambda_{nm}, 0, p) = 0$, in the non-simplified eq. (3.1). The result is that we now have starting points for almost all spectral curves $\lambda_j(k)$ that exist for $k = 0$[1]. There are two additional roots $\lambda = -v, -rv$ that are the result of cancellation in producing P.

For example, for the second order $\hat{L}$ in eq. (1.10), we have 24 potential solutions from the polynomials, within which there are all but two of the solutions that exist for $k = 0$. This method is used because finding all roots of polynomials is much more predictable (we know how many roots there will be) than finding all roots of a general nonlinear function such as eq. (3.1).

3.2 Computation of spectral curves

From the solutions $\lambda_j(0)$, we can compute $\lambda_j(k)$ using parameter continuation in k. There are a couple of places where the continuation algorithm needs to be modified slightly: when branches of solutions intersect at a given $k = k_r$ (resonant) value, resulting in a repeated root, and then split off, potentially non-smoothly, for k less than or greater than this value. The case where eigenvalues go through a resonant splitting from 2 complex pairs to 2 other complex pairs seems to be handled fine by the basic continuation algorithm, but resonance involving $\mathbb{R} \to \mathbb{C}$ or $\mathbb{C} \to \mathbb{R}$ need some modification to be handled reliably.

3.2.1 Continuation

Computation of the curves $\lambda_j(k)$ is done through simple parameter continuation in k. Since we don't need to consider folds with respect to k, this is sufficient. We write the spectrum in terms of its real and imaginary parts, $\lambda = \mu + i\omega$, and split the original equation (3.1) into an equation for its real and its imaginary parts

$$\begin{aligned} G(\mu, \omega, k, p) &= \operatorname{Re} F(\mu + i\omega, k, p) = 0, \\ H(\mu, \omega, k, p) &= \operatorname{Im} F(\mu + i\omega, k, p) = 0. \end{aligned} \tag{3.5}$$

For a given k, we can approximate $\lambda(k + \Delta k)$ using a Newton iteration of the form $\lambda^{n+1}(k + \Delta k) = \lambda^n - \Delta\lambda^n$, where the the superscript denotes the iteration number. $\Delta\lambda = \Delta\mu + i\Delta\omega$ is given by

$$\begin{pmatrix} \Delta\mu^n \\ \Delta\omega^n \end{pmatrix} = \begin{pmatrix} G_\mu(\mu^n, \omega^n, k + \Delta k, p) & G_\omega(\mu^n, \omega^n, k + \Delta k, p) \\ H_\mu(\mu^n, \omega^n, k + \Delta k, p) & H_\omega(\mu^n, \omega^n, k + \Delta k, p) \end{pmatrix}^{-1} \begin{pmatrix} G(\mu^n, \omega^n, k + \Delta k, p) \\ H(\mu^n, \omega^n, k + \Delta k, p) \end{pmatrix}. \tag{3.6}$$

And this is iterated until either the norm of update, or the norm of residual falls below some tolerance `TOL`. The partial derivatives found in the Jacobian (and even the functions G and H themselves) are very ugly symbolically, but we have found that numerical evaluation (in Maple)

[1] We haven't determined a way to guarantee finding solutions $\lambda_j(k)$ that exist only on some interval $0 < k_1 < k < k_2$

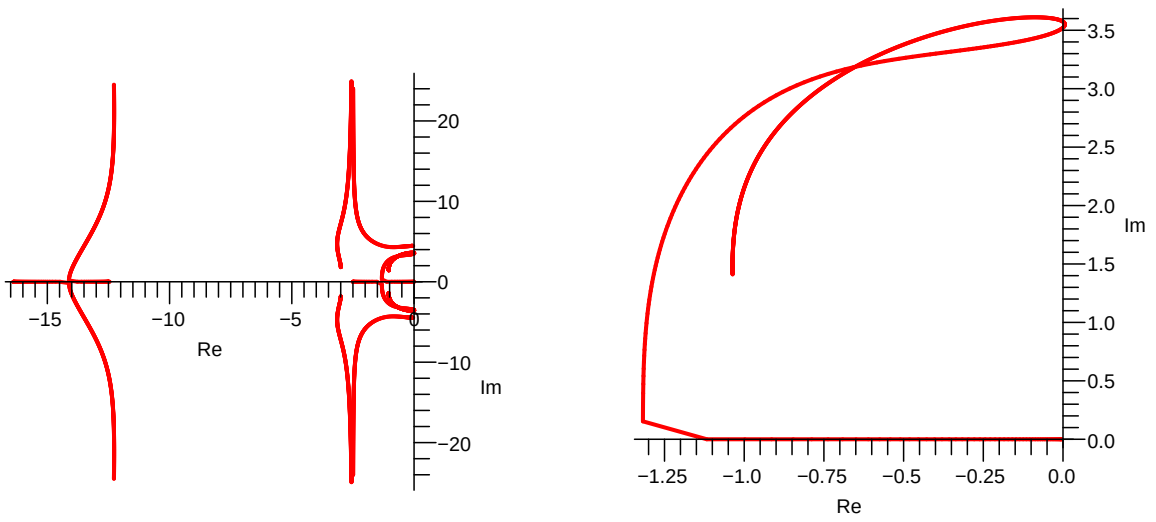

Figure 3.1: Spectrum for parameters $v = 2.5, r = 5, \gamma_1 = 0.92, a_e = 26, a_i = 25, \alpha = 2$, and $\tilde{\eta}(\lambda) = \left(\lambda^2 + \alpha\lambda + 1\right)^{-1}$. This parameter set leads to a very small band (in k) of unstable oscillatory modes, i.e., just beyond a dynamic Turing bifurcation. Left: full spectrum computed for $k \in [0, 20]$. Right: Just the branch causing the bifurcation. $\lambda(k = 0)$ starts on the real line, and eventually goes through a resonance to become complex as k increases.

only at the points where they need to be computed is quite reliable. This allows us to easily compute to a tolerance of $\texttt{TOL} = 10^{-(\texttt{Digits}-4)}$, with `Digits` the current set precision in Maple. With this setup, computing solutions with `Digits` $= 40$ or more is no problem due to the quadratic convergence of Newton's method.

3.2.2 Resonant splitting

We use this term to describe the collision of two branches of the spectrum at a given k value, denoted k_r. There are 3 possibilities for this happening.

From real axis to complex plane

Sometimes we have a situation where two branches in the spectrum are moving towards each other on the real line. At k_r, they form a double root, and then split off into a complex pair for $k > k_r$. This can be detected by a loss of convergence of Newton's method, as once the roots have split, the initial (real) approximation to the root will never move off of the real line. Once detected, this can be remedied by perturbing each branch with a finite non-zero imaginary amount. For consistency, we perturb branches with positive imaginary value if they were previously decreasing, and negative imaginary value if increasing. This behaviour is seen in all of the spectra we have computed so far, for example there are two occurrences of this in fig. 3.1 and 1 occurrence in fig. 3.2.

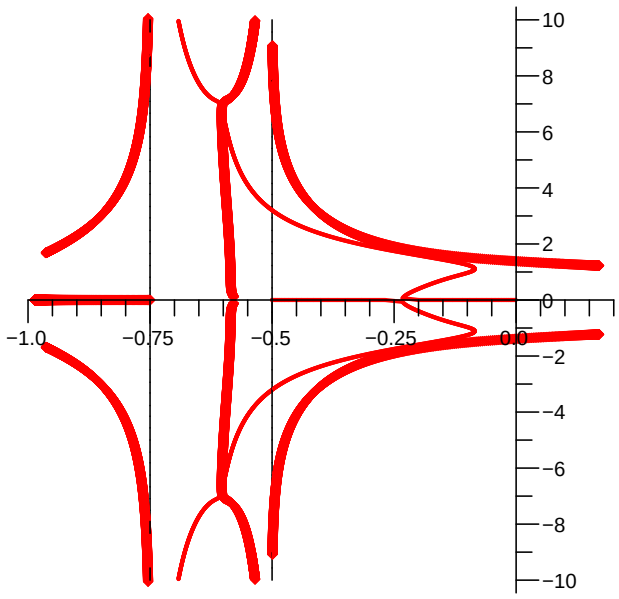

Figure 3.2: Complex spectrum for parameters $v = 0.5, r = 1.5, \gamma_1 = 0.97, a_e = 26, a_i = 25, \alpha = 2$, and $\tilde{\eta}(\lambda) = \left(\lambda^2 + \gamma\lambda + 1\right)^{-1}$. This diagram displays a $\mathbb{C} \to \mathbb{C}$ resonant splitting at about $-0.6 \pm 8i$.

From complex plane to real axis

The opposite of the previous case. Two branches which are complex conjugates for $k < k_r$ meet at $k = k_r$ and then move away from each other on the real line for $k > k_r$. This can be handled in a similar way to the previous case, with small, consistent, perturbations when Newton convergence wanes. This comes up very often for $\alpha > 2$ as looking at asymptotics for $k \to \infty$ reveals two distinct, negative, finite real roots.

From complex plane to complex plane

Nothing seems to need to be done here, we have observed a couple of cases where the standard Newton iteration captures this splitting just fine. A problem can happen if we get unlucky and have $k = k_r$ at some point in the discretized continuation, but this is an unlikely scenario, and it can be handled with how the Newton iteration is initialized. An example of a spectrum with this happening can be seen in fig. 3.2.

3.3 Continuation of branch maxima

To continue the (real part) maximal points of a branch of spectrum, i.e., the right most part of the loop in the right image in fig. 3.1, we need to add another equation to the eqs. (3.5) that corresponds to $\mu'(k) = \mu'(\omega) = 0$. This gives us the system

$$\begin{aligned} G(\mu, \omega, k, p) &= \operatorname{Re} F(\mu + i\omega, k, p) = 0 \\ H(\mu, \omega, k, p) &= \operatorname{Im} F(\mu + i\omega, k, p) = 0 \\ J(\mu, \omega, k, p) &= G_k H_\omega - G_\omega H_k = 0 \end{aligned} \tag{3.7}$$

The idea here is to perform continuation in one of the additional parameters, say $p_1 = \gamma_1$, and the solutions along this continuation line give us the maximal points $\mu_{max}, \omega_{max}, k_{max}$ for some p_1. We perform this continuation until we find a solution with $\mu_{max} \approx 0$, and then we switch our viewpoint again.

3.4 Continuation of critical point

Now we can finally consider the refinement and continuation of critical points. That is, the points that cause Turing and dynamic Turing bifurcations with $k_c \neq 0$. This requires us to look at solutions to the system

$$\begin{aligned} G(0, \omega, k, p) &= \operatorname{Re} F(i\omega, k, p) = 0 \\ H(0, \omega, k, p) &= \operatorname{Im} F(i\omega, k, p) = 0 \\ J(0, \omega, k, p) &= G_k H_\omega - G_\omega H_k = 0 \end{aligned} \tag{3.8}$$

In terms of ω, k and a parameter p_1. To do so, we perform continuation in yet another parameter, p_2 to obtain ω_c, k_c for some p_1, p_2.

In general, this and the previous section would benefit from pseudo-arclength continuation as monotonicity in a given parameter can not be assumed as it was for k. We have not implemented this with our Maple code, but have got along fine finding and continuing dynamic Turing bifurcations using parameter continuation for some parameter regimes.

3.5 Summary

The steps taken to find a dynamic Turing bifurcation go as follows:

1. Set paramaters and compute the full spectrum for some range of k values, $k \in [0, k_{max}]$.
2. Find the point that has maximal μ, and nonzero ω and k.
3. Perform continuation of the found point using eq. (3.7) until you find $\mu_{max} \approx 0$.
4. Refine (and potentially continue in another parameter) the solution using eq. (3.8).

The result is that you will have a set of paramaters, and a k_c and ω_c where a dynamic Turing instability occurs. Whether this is a primary instability depends on the other branches of the spectrum, so a quick computation of the spectrum at the new parameter values is recommended to check.

Chapter 4

Normal form for dynamic square tiling patterns

This chapter serves to show how a Hopf bifurcation with nonzero wave number (dynamic Turing bifurcation) of the 2D neural field equation with finite transmission speed on a periodic square domain maps to the normal form analyzed in Silber and Knobloch [15]. The method for doing so is extended from the 1D case presented in Venkov et al. [16], where separation of scales is applied. The resulting normal form is $\mathbb{C}^4$ dimensional, and admits at least 5 different types of periodic solutions branching from the bifurcation, depending on the normal form paramaters.

Note that this chapter only discusses the $D_4 \ltimes T^2$ tiling pattern, the semidirect product of the (discrete) dihedral group D_4 and the continuous group of translations in 2D T^2. The only other possible tiling patterns in two-dimensional space are rhomboid ($D_2 \ltimes T^2$) and hexagonal ($D_6 \ltimes T^2$).

4.1 Separation of scales

To do weakly nonlinear analysis of the model, we need to Taylor expand the firing function f beyond the linear term that was used in eq. (2.2),

$$f(u) = f(u_0) + \gamma_1 (u - u_0) + \gamma_2 (u - u_0)^2 + \gamma_3 (u - u_0)^3 + \mathcal{O}\left((u - u_0)^4\right), \tag{4.1}$$

with $\gamma_n = f^{(n)}(u_0)/n!$, its derivatives evaluated at the homogeneous equilibrium.

Just beyond a dynamic Turing bifurcation, we will see the slow growth of the dominant eigenmodes. This leads naturally to the idea of identifying different time scales in the system. The behaviour that occurs at all but the slowest of time scales can be discarded to obtain information about the envelopes, or 'amplitudes', of the slowest scale.

If we Taylor expand the dispersion curve (2.6) at the maximum, we can obtain $\mu \sim \gamma_1 - \gamma_c$ and $k - k_c \sim \sqrt{\gamma_1 - \gamma_c}$ near the dynamic Turing bifurcation, where γ_1 is the bifurcation parameter, and γ_c the value of γ_1 at bifurcation. For $\gamma_1 > \gamma_c$, emergent patterns can thus be written as an infinite sum of unstable modes of the form $e^{\mu_0(\gamma_1-\gamma_c)} e^{i\sqrt{\gamma_1-\gamma_c}\mathbf{k}_0\cdot\mathbf{x}} e^{i(\omega_c t + \mathbf{k}_c\cdot\mathbf{x})}$, with μ_0 and $\mathbf{k}_0$ some unknown constants in the proportionalities. If we define $\delta \equiv (\gamma_1 - \gamma_c)/\epsilon^2$, and take ϵ small, then we can identify the fast eigenmodes as $e^{i(\omega_c t + \mathbf{k}_c\cdot\mathbf{x})}$, and the slow modulations of the form $e^{\mu_0\epsilon^2 t} e^{i\epsilon\mathbf{k}_0\cdot\mathbf{x}}$.

We define scaled parameters, $\boldsymbol{\chi} = \epsilon\mathbf{x}$ and $\tau = \epsilon^2 t$ according to this reasoning, and also include an intermediate time scale $\theta = \epsilon t$ (which is needed to 'step through' some integrals in the perturbative

analysis), to finally write solutions in the form $A(\boldsymbol{\chi}, \theta, \tau)e^{i(\omega_c t + \mathbf{k}_c \cdot \mathbf{x})}$, with A containing everything we do not know about the slow scales.

Now, we take a perturbation of the solution to the model eq. (1.5) in the form

$$u\left(\mathbf{x}, t\right) - u_0 = \sum_{n=1}^{\infty} \epsilon^n u_n\left(\mathbf{x}, t, \boldsymbol{\chi}, \theta, \tau\right). \tag{4.2}$$

Placing each order of this expansion into the model separately results in

$$u_n\left(\mathbf{x}, t, \boldsymbol{\chi}, \theta, \tau\right) = M_0 u_n + \epsilon M_1 u_n + \epsilon^2 M_2 u_n + \mathcal{O}(\epsilon^3) \tag{4.3}$$

with the operators M_i defined as

$$\begin{aligned}
M_0 =& \eta * K \otimes, \\
M_1 =& -\eta * \left(x_1 K \otimes \frac{\partial}{\partial \chi_1} + x_2 K \otimes \frac{\partial}{\partial \chi_2} \right) - \left(t\eta * K + \eta * tK \right) \otimes \frac{\partial}{\partial \theta}, \\
M_2 =& \frac{1}{2}\eta * \left(x_1^2 K \otimes \frac{\partial^2}{\partial \chi_1^2} + x_2^2 K \otimes \frac{\partial^2}{\partial \chi_2^2} \right) + \eta * x_1 x_2 K \otimes \frac{\partial}{\partial \chi_1}\frac{\partial}{\partial \chi_2} \\
&+ t\eta * \left(x_1 K \otimes \frac{\partial}{\partial \chi_1} + x_2 K \otimes \frac{\partial}{\partial \chi_2} \right) \frac{\partial}{\partial \theta} \\
&+ \eta * t \left(x_1 K \otimes \frac{\partial}{\partial \chi_1} + x_2 K \otimes \frac{\partial}{\partial \chi_2} \right) \frac{\partial}{\partial \theta} \\
&+ \frac{1}{2}\left(t^2 \eta * K + 2t\eta * tK + \eta * t^2 K \right) \otimes \frac{\partial^2}{\partial \theta^2} \\
&+ \left(t\eta * K + \eta * tK \right) \otimes \frac{\partial}{\partial \tau}.
\end{aligned} \tag{4.4}$$

Looking at the model equation (1.5) using this expansion, we can pull out the equations for each order of ϵ

$$\begin{aligned}
\left(1 - \gamma_c M_0\right) u_1 &= g_1 = 0, \\
\left(1 - \gamma_c M_0\right) u_2 &= g_2 = \gamma_2 M_0 u_1^2 + \gamma_c M_1 u_1, \\
\left(1 - \gamma_c M_0\right) u_3 &= g_3 = M_0\left(2\gamma_2 u_1 u_2 + \gamma_3 u_1^3 + \delta u_1\right) + M_1\left(\gamma_c u_2 + \gamma_2 u_1^2\right) + \gamma_c M_2 u_1.
\end{aligned} \tag{4.5}$$

Notice how the left hand side always has the same operator, which we define as

$$\mathcal{L} \equiv 1 - \gamma_c M_0, \tag{4.6}$$

and the right hand side contains only elements that can be computed in the row above, $g_n = g_n(u_1, u_2, \ldots, u_{n-1})$. With this view, it becomes clear that solutions built up in this way are in the form of perturbations of the nullspace of $\mathcal{L}$.

If we restrict ourselves to looking at a square periodic domain of length $2\pi/k_c$, then it follows that $u_1 \in \ker \mathcal{L}$ can be expressed as

$$u_1 = \sum_{i=1}^{4} \left(A_i \phi_i + \bar{A}_i \bar{\phi}_i \right) \tag{4.7}$$

with the basis functions (the critical eigenmodes at bifurcation)

$$\begin{aligned}\phi_1 &= e^{i(\omega_c t + k_c x_1)},\\ \phi_2 &= e^{i(\omega_c t - k_c x_1)},\\ \phi_3 &= e^{i(\omega_c t + k_c x_2)},\\ \phi_4 &= e^{i(\omega_c t - k_c x_2)},\end{aligned} \tag{4.8}$$

and the bar denoting complex conjugation.

The unknowns in the problem are now the amplitudes $A_i(\boldsymbol{\chi}, \theta, \tau)$, which are functions of the scaled parameters. Due to how the perturbation solutions are structured, the Fredholm alternative can be applied to find equations for these amplitudes.

4.2 Fredholm alternative

The form of the perturbation expansion is $\mathcal{L}u_n = g_n(u_1, u_2, \ldots, u_{n-1})$, such that the right hand side always contains known quantities. Thus to construct solutions that are a finite truncation of the system, we just need to know the inverse of $\mathcal{L}$. The Fredholm alternative may be applied [17] to put solvability conditions on the g_n, which will lead to conditions on the amplitudes.

Considering the basis on the square periodic domain that we have already written, eq. (4.7), we notice that this solution is also periodic in time. Thus, we are concerning ourselves with the domain $\Lambda = [0, 2\pi/k_c]^2 \times [0, 2\pi/\omega_c]$. To apply the Fredholm alternative, we define the inner product to be

$$\langle u, v\rangle = \frac{k_c^2 \omega_c}{8\pi^3} \int_\Lambda \mathrm{d}\mathbf{x}\mathrm{d}t\, \bar{u}(\mathbf{x}, t) v(\mathbf{x}, t). \tag{4.9}$$

This definition is chosen such that our basis for the nullspace (4.8) is orthonormal, $\langle \phi_i, \phi_j\rangle = \delta_{ij}$.

Under this inner product, the adjoint to $\mathcal{L}$ is given by $\mathcal{L}^* = 1 - \gamma_c \eta(-t) * K(\mathbf{x}, -t)\otimes$. Since the dispersion relation is invariant under time reversal $t \to -t$, $\mathcal{L}$ and $\mathcal{L}^*$ have the same nullspace.

The Fredholm alternative states that for all $u \in \ker \mathcal{L}$, it must hold that $\langle u, g_n\rangle = \langle u, \mathcal{L}u_n\rangle = \langle \mathcal{L}^* u, u_n\rangle = 0$. This means that deriving equations for the amplitudes can be accomplished simply by computing the inner products

$$\langle \phi_i, g_n\rangle = 0, \quad i = 1 \ldots 4. \tag{4.10}$$

For the first nontrivial equation, and looking specifically at ϕ_1, we obtain

$$\begin{aligned}\langle \phi_1, g_2\rangle = 0 &= \gamma_2 \langle \phi_1, M_0 u_1^2\rangle + \gamma_c \langle \phi_1, M_1 u_1\rangle\\ &= \gamma_2 \tilde{\eta}\widehat{K}\langle \phi_1, u_1^2\rangle + \gamma_c \left(-\tilde{\eta}\frac{\partial}{\partial i k_1}\frac{\partial}{\partial \chi_1}\widehat{K} + \frac{\partial}{\partial i\omega}\frac{\partial}{\partial \theta}\tilde{\eta}\widehat{K}\right)\langle \phi_1, u_1\rangle\\ &= \left(-\tilde{\eta}\frac{\partial}{\partial i k_1}\frac{\partial}{\partial \chi_1}\widehat{K} + \frac{\partial}{\partial i\omega}\frac{\partial}{\partial \theta}\tilde{\eta}\widehat{K}\right) A_1\\ &= \left(\frac{\partial}{\partial \theta} - v_{g1}\frac{\partial}{\partial \chi_1}\right) A_1\end{aligned} \tag{4.11}$$

where $v_{g1} = \partial\omega/\partial k_1|_{\mathbf{k}=(k_c,0)^T}$ can be considered a group velocity, and the Laplace and Fourier-Laplace transforms are evaluated at the critical arguments. Going from the 2nd to 3rd lines in

(4.11) makes use of $\langle \phi_i, u_1^2 \rangle = 0$, and $\langle \phi_i, u_1 \rangle = A_i$. The final line of (4.11) has a solution that restricts how A_1 depends on its arguments. Doing a similar thing with the other basis functions leads to restrictions on all of the amplitudes

$$\begin{aligned}
A_1(\boldsymbol{\chi}, \theta, \tau) &= A_1(\chi_1 + v_{g1}\theta, \chi_2, \tau) \equiv A_1(\xi_1, \chi_2, \tau) \\
A_2(\boldsymbol{\chi}, \theta, \tau) &= A_2(\chi_1 - v_{g1}\theta, \chi_2, \tau) \equiv A_2(\xi_2, \chi_2, \tau) \\
A_3(\boldsymbol{\chi}, \theta, \tau) &= A_3(\chi_1, \chi_2 + v_{g2}\theta, \tau) \equiv A_3(\chi_1, \xi_3, \tau) \\
A_4(\boldsymbol{\chi}, \theta, \tau) &= A_4(\chi_1, \chi_2 - v_{g2}\theta, \tau) \equiv A_4(\chi_1, \xi_4, \tau),
\end{aligned} \tag{4.12}$$

where $v_{g2} = \partial\omega/\partial k_2|_{\mathbf{k}=(0,k_c)^T} = v_{g1} \equiv v_g$.

Calculating $\langle \phi_i, g_3 \rangle$ requires much more work. In particular, there is the inner product $\langle \phi_i, u_1^3 \rangle$ which requires the cube of the assumed solution (4.7) (64 terms before simplification), and then there are $\langle \phi_1, u_2 \rangle$ and $\langle \phi_i, u_1 u_2 \rangle$ which both require an expression for u_2 before they can be evaluated. Looking again just at ϕ_1, with some manipulation, we eventually come to

$$\begin{aligned}
\langle \phi_1, g_3 \rangle = 0 = {} & 2\gamma_2 \tilde{\eta} \widehat{K} \langle \phi_1, u_1 u_2 \rangle + \gamma_3 \tilde{\eta} \widehat{K} \langle \phi_1, u_1^3 \rangle + \delta \tilde{\eta} \widehat{K} \langle \phi_1, u_1 \rangle + \\
& + \gamma_c \left(-\frac{\partial}{\partial i k_1} \frac{\partial}{\partial \chi_1} + \frac{\partial}{\partial i\omega} \frac{\partial}{\partial \theta} \right) \tilde{\eta} \widehat{K} \langle \phi_1, u_2 \rangle + \\
& + \gamma_c \left[\frac{1}{2} \left(-\frac{\partial}{\partial i k_1} \frac{\partial}{\partial \chi_1} + \frac{\partial}{\partial i\omega} \frac{\partial}{\partial \theta} \right)^2 + \frac{\partial}{\partial i\omega} \frac{\partial}{\partial \tau} \right] \tilde{\eta} \widehat{K} \langle \phi_1, u_1 \rangle.
\end{aligned} \tag{4.13}$$

It must be noted that the differential operators (both here and in eq. (4.11)) that appear will change when the basis function we are computing with changes.

To obtain u_2, notice that the equation for it in (4.5) contains only linear operators, such that u_2 will be a quadratic form of the basis functions. Writing it as

$$u_2 = \sum_{l,m,n=\{0,\pm1,\pm2\}} B_{lmn} e^{i(l\omega_c t + m k_c x_1 + n k_c x_2)}, \tag{4.14}$$

and subbing it into the relevant equation of (4.5) will let us work out the coefficients B_{lmn}. This approach will work for all coefficients except for $\{B_{l0m}, B_{lm0} | l, m = \pm 1\}$ which can't be determined because their corresponding modes lie in $\ker \mathcal{L}$. These coefficients that can't be determined remain as functions of $(\xi_1, \xi_2, \xi_3, \xi_4, \tau)$.

The inner products in (4.13) (ordered by how easy they were to compute) are

$$\begin{aligned}
\langle \phi_1, u_1 \rangle &= A_1 \\
\langle \phi_1, u_2 \rangle &= B_{110} \\
\langle \phi_1, u_1^3 \rangle &= 3A_1 \left(|A_1|^2 + 2|A_2|^2 + 2|A_3|^2 + 2|A_4|^2 \right) + 6\bar{A}_2 A_3 A_4 \\
\langle \phi_1, u_1 u_2 \rangle &= A_1 [(2C_{000} + C_{220}) |A_1|^2 + 2(C_{200} + C_{020} + C_{000}) |A_2|^2 + \\
&\quad + 2(C_{211} + C_{011} + C_{000}) |A_3|^2 + 2(C_{000} + C_{011} + C_{211}| A_4|^2] + \\
&\quad + 2(2C_{011} + C_{200}) \bar{A}_2 A_3 A_4
\end{aligned} \tag{4.15}$$

with the shorthand notation

$$C_{lmn} = \frac{\tilde{\eta}(il\omega_c) \widehat{K}((mk_c, nk_c)^T, il\omega_c)}{1 - \gamma_c \tilde{\eta}(il\omega_c) \widehat{K}((mk_c, nk_c)^T, il\omega_c)}. \tag{4.16}$$

Subbing these inner products into eq. (4.13), we are left with the problem of how the differential operator acts on B_{110},

$$\left(-\frac{\partial}{\partial ik_1}\frac{\partial}{\partial \chi_1}+\frac{\partial}{\partial i\omega}\frac{\partial}{\partial \theta}\right)\tilde{\eta}\widehat{K}B_{110}=\left[-2\frac{\partial(\tilde{\eta}\widehat{K})}{\partial ik_1}\frac{\partial}{\partial \xi_2}+\frac{\partial(\tilde{\eta}\widehat{K})}{\partial ik_2}\left(\frac{\partial}{\partial \xi_3}-\frac{\partial}{\partial \xi_4}\right)\right]B_{110} \tag{4.17}$$

by the chain rule. Finally, applying the operators to A_1 results in

$$\begin{aligned}\left[\frac{1}{2}\left(-\frac{\partial}{\partial ik_1}\frac{\partial}{\partial \chi_1}+\frac{\partial}{\partial i\omega}\frac{\partial}{\partial \theta}\right)^2+\frac{\partial}{\partial i\omega}\frac{\partial}{\partial \tau}\right]\tilde{\eta}\widehat{K}A_1 = \\ \frac{1}{2}\left(-\frac{\partial}{\partial ik_1}+v_g\frac{\partial}{\partial i\omega}\right)^2\left(\tilde{\eta}\widehat{K}\right)\frac{\partial^2 A_1}{\partial \xi_1^2}+\frac{\partial(\tilde{\eta}\widehat{K})}{\partial i\omega}\frac{\partial A_1}{\partial \tau}\end{aligned} \tag{4.18}$$

again by simple application of the chain rule.

Notice how eq. (4.17) shows that only derivatives in ξ_2, ξ_3, and ξ_4 of the unknown quantity B_{110} will occur in the final result. These are now eliminated by an averaging procedure. If we average the resulting equation over ξ_2, ξ_3, and ξ_4, then derivatives of the averaged $\langle B_{110}\rangle$, will vanish, and we can write the final equation for the amplitude A_1 as

$$\begin{aligned}\frac{\partial A_1}{\partial \tau} = a_0A_1+A_1\left[a_1\langle|A_2|^2\rangle_2+a_2\left(|A_1|^2+\langle|A_2|^2\rangle_2\right)+a_3\left(\langle|A_3|^2\rangle_3+\langle|A_4|^2\rangle_4\right)\right]+ \\ +a_4\langle\bar{A}_2\rangle_2\langle A_3\rangle_3\langle A_4\rangle_4+a_5\frac{\partial^2 A_1}{\partial \xi_1^2},\end{aligned} \tag{4.19}$$

with parameters given by

$$\begin{aligned}a_0 &= -\frac{\delta}{\gamma_c^2}\left(\frac{\partial(\tilde{\eta}\widehat{K})}{\partial i\omega}\right)^{-1} \\ a_1 &= -\frac{1}{\gamma_c^2}\left(\frac{\partial(\tilde{\eta}\widehat{K})}{\partial i\omega}\right)^{-1}\left[2\gamma_2^2\left(2C_{200}+2C_{020}-C_{220}\right)+3\gamma_3\right] \\ a_2 &= -\frac{1}{\gamma_c^2}\left(\frac{\partial(\tilde{\eta}\widehat{K})}{\partial i\omega}\right)^{-1}\left[2\gamma_2^2\left(2C_{000}+C_{220}\right)+3\gamma_3\right] \\ a_3 &= -\frac{1}{\gamma_c^2}\left(\frac{\partial(\tilde{\eta}\widehat{K})}{\partial i\omega}\right)^{-1}\left[4\gamma_2^2\left(C_{211}+C_{011}+C_{000}\right)+6\gamma_3\right] \\ a_4 &= -\frac{1}{\gamma_c^2}\left(\frac{\partial(\tilde{\eta}\widehat{K})}{\partial i\omega}\right)^{-1}\left[4\gamma_2^2\left(2C_{011}+C_{200}\right)+6\gamma_3\right], \\ a_5 &= -\frac{1}{2}\left(\frac{\partial(\tilde{\eta}\widehat{K})}{\partial i\omega}\right)^{-1}\left(\frac{\partial}{\partial ik_1}-v_g\frac{\partial}{\partial i\omega}\right)^2\left(\tilde{\eta}\widehat{K}\right)\end{aligned} \tag{4.20}$$

and the subscript on the average brackets indicating which ξ_i is being averaged over. For example, we can consider periodically varying amplitudes, and define our averages as

$$\langle Y\rangle_i=\frac{1}{P_i}\int_0^{P_i}Y\mathrm{d}\xi_i \tag{4.21}$$

where P_i is the period in the ξ_i dimension.

Through similar computations, equations for the other amplitudes can be derived as well.

$$\begin{aligned}\frac{\partial A_2}{\partial \tau} = a_0 A_2 + A_2 \left[a_1 \langle |A_1|^2 \rangle_1 + a_2 \left(\langle |A_1|^2 \rangle_1 + |A_2|^2\right) + a_3 \left(\langle |A_3|^2 \rangle_3 + \langle |A_4|^2 \rangle_4\right)\right] + \\ + a_4 \langle \bar{A}_1 \rangle_1 \langle A_3 \rangle_3 \langle A_4 \rangle_4 + a_5 \frac{\partial^2 A_2}{\partial \xi_2^2}\end{aligned} \tag{4.22}$$

$$\begin{aligned}\frac{\partial A_3}{\partial \tau} = a_0 A_3 + A_3 \left[a_1 \langle |A_4|^2 \rangle_4 + a_2 \left(|A_3|^2 + \langle |A_4|^2 \rangle_4\right) + a_3 \left(\langle |A_1|^2 \rangle_1 + \langle |A_2|^2 \rangle_2\right)\right] + \\ + a_4 \langle \bar{A}_4 \rangle_4 \langle A_1 \rangle_1 \langle A_2 \rangle_2 + a_5 \frac{\partial^2 A_3}{\partial \xi_3^2}\end{aligned} \tag{4.23}$$

$$\begin{aligned}\frac{\partial A_4}{\partial \tau} = a_0 A_4 + A_4 \left[a_1 \langle |A_3|^2 \rangle_3 + a_2 \left(\langle |A_3|^2 \rangle_3 + |A_4|^2\right) + a_3 \left(\langle |A_1|^2 \rangle_1 + \langle |A_2|^2 \rangle_2\right)\right] + \\ + a_4 \langle \bar{A}_3 \rangle_3 \langle A_1 \rangle_1 \langle A_2 \rangle_2 + a_5 \frac{\partial^2 A_4}{\partial \xi_4^2}\end{aligned} \tag{4.24}$$

Noting how the a_i parameters come into play in each equation. The equations have been written in their particular form to facilitate the next section.

4.3 $D_4 \ltimes T^2$ Normal form

Ignoring the ξ_i dependence of the amplitude equations leads to the system

$$\begin{aligned}\frac{\mathrm{d}A_1}{\mathrm{d}\tau} &= a_0 A_1 + A_1 \left[a_1 |A_2|^2 + a_2 \left(|A_1|^2 + |A_2|^2\right) + a_3 \left(|A_3|^2 + |A_4|^2\right)\right] + a_4 \bar{A}_2 A_3 A_4 \\ \frac{\mathrm{d}A_2}{\mathrm{d}\tau} &= a_0 A_2 + A_2 \left[a_1 |A_1|^2 + a_2 \left(|A_1|^2 + |A_2|^2\right) + a_3 \left(|A_3|^2 + |A_4|^2\right)\right] + a_4 \bar{A}_1 A_3 A_4 \\ \frac{\mathrm{d}A_3}{\mathrm{d}\tau} &= a_0 A_3 + A_3 \left[a_1 |A_4|^2 + a_2 \left(|A_3|^2 + |A_4|^2\right) + a_3 \left(|A_1|^2 + |A_2|^2\right)\right] + a_4 \bar{A}_4 A_1 A_2 \\ \frac{\mathrm{d}A_4}{\mathrm{d}\tau} &= a_0 A_4 + A_4 \left[a_1 |A_3|^2 + a_2 \left(|A_3|^2 + |A_4|^2\right) + a_3 \left(|A_1|^2 + |A_2|^2\right)\right] + a_4 \bar{A}_3 A_1 A_2.\end{aligned} \tag{4.25}$$

This is the normal form for the Hopf bifurcation on a square lattice that is determined and analyzed in Silber & Knobloch [15], with slight differences:

- Each equation does not have a $i\omega_c A_i$ term in it, because we have incorporated that into our basis functions.
- We have $a_0 \propto \delta$, the distance away from the bifurcation, but the scaling seems to be different from that in [15]. This shouldn't affect existence and stability of the periodic branches that originate here.
- The negative sign in front of delta may affect the stability and criticality of bifurcating solutions. It is not entirely clear yet, but if this is the case, taking $\tau \to -\tau$ may fix it.

Details of the calculations in this chapter will be written elsewhere, along with the process of how to actually make use of eq. (4.25).

Bibliography

[1] S. Amari, "Homogeneous nets of neuron-like elements.," *Biological cybernetics*, vol. 17, pp. 211–20, Jan. 1975.

[2] P. Nunez, "The brain wave equation: A model for the EEG," *Math Biosci*, vol. 21, pp. 279–297, 1974.

[3] V. Jirsa and H. Haken, "A derivation of a macroscopic field theory of the brain from the quasi-microscopic neural dynamics," *Physica D: Nonlinear Phenomena*, vol. 99, no. 4, pp. 503–526, 1997.

[4] A. Hutt and F. M. Atay, "Analysis of nonlocal neural fields for both general and gamma-distributed connectivities," *Physica D: Nonlinear Phenomena*, vol. 203, pp. 30–54, Apr. 2005.

[5] H. R. Wilson and J. D. Cowan, "Excitatory and Inhibitory Interactions in Localized Populations of Model Neurons," *Biophys J*, vol. 12, no. 1, pp. 1–24, 1972.

[6] P. C. Bressloff, "Traveling fronts and wave propagation failure in an inhomogeneous neural network," *Physica D: Nonlinear Phenomena*, vol. 155, pp. 83–100, July 2001.

[7] Z. P. Kilpatrick, S. E. Folias, and P. C. Bressloff, "Traveling Pulses and Wave Propagation Failure in Inhomogeneous Neural Media," *SIAM Journal on Applied Dynamical Systems*, vol. 7, pp. 161–185, Jan. 2008.

[8] A. Hutt, M. Bestehorn, and T. Wennekers, "Pattern formation in intracortical neuronal fields.," *Network (Bristol, England)*, vol. 14, pp. 351–68, May 2003.

[9] M. Abramowitz, I. A. Stegun, and D. Miller, "Handbook of Mathematical Functions With Formulas, Graphs and Mathematical Tables (National Bureau of Standards Applied Mathematics Series No. 55)," 1965.

[10] I. S. Gradshteyn, I. M. Ryzhik, A. Jeffrey, Y. V. Geronimus, M. Y. Tseytlin, and Y. C. Fung, "Table of Integrals, Series, and Products," 1981.

[11] E. J. Nichols and A. Hutt, "Neural field simulator: fast computation and 3D-visualization," *BMC Neuroscience*, vol. 14(1), 2013.

[12] A. Hutt and N. Rougier, "Activity spread and breathers induced by finite transmission speeds in two-dimensional neural fields," *Phys Rev E*, vol. 82, p. 055701, Nov. 2010.

[13] A. M. Turing, "The Chemical Basis of Morphogenesis," *Philosophical Transactions of the Royal Society B: Biological Sciences*, vol. 237, pp. 37–72, Aug. 1952.

[14] F. M. Atay and A. Hutt, "Stability and Bifurcations in Neural Fields with Finite Propagation Speed and General Connectivity," 2004.

[15] M. Silber and E. Knobloch, "Hopf bifurcation on a square lattice," *Nonlinearity*, vol. 4, pp. 1063–1107, Nov. 1991.

[16] N. Venkov, S. Coombes, and P. Matthews, "Dynamic instabilities in scalar neural field equations with space-dependent delays," *Physica D: Nonlinear Phenomena*, vol. 232, pp. 1–15, Aug. 2007.

[17] G. Helmberg, *Introduction to spectral theory in hilbert space*. Amsterdam: North Holland Publishing Company, 1969.